PHYSICAL REVIEW B **84**, 235120 (2011)

Electronic structure of EuN: Growth, spectroscopy, and theory

J. H. Richter,[1] B. J. Ruck,[1,*] M. Simpson,[1] F. Natali,[1] N. O. V. Plank,[1] M. Azeem,[1] H. J. Trodahl,[1] A. R. H. Preston,[2] B. Chen,[2] J. McNulty,[2] K. E. Smith,[2] A. Tadich,[3] B. Cowie,[3] A. Svane,[4] M. van Schilfgaarde,[5] and W. R. L. Lambrecht[6]

[1]*The MacDiarmid Institute for Advanced Materials and Nanotechnology, School of Chemical and Physical Sciences, Victoria University of Wellington, P.O. Box 600, Wellington 6140, New Zealand*

[2]*Department of Physics, Boston University, 590 Commonwealth Avenue, Boston, Massachusetts 02215, USA*

[3]*Australian Synchrotron, Clayton, Victoria 3168, Australia*

[4]*Department of Physics and Astronomy, Aarhus University, DK-8000 Aarhus C, Denmark*

[5]*School for Engineering of Matter, Transport and Energy, Arizona State University, Tempe, Arizona 85287, USA*

[6]*Department of Physics, Case Western Reserve University, Cleveland, Ohio 44106, USA*

(Received 29 August 2011; published 6 December 2011)

We present a detailed study of the electronic structure of europium nitride (EuN), comparing spectroscopic data to the results of advanced electronic structure calculations. We demonstrate the epitaxial growth of EuN films, and show that in contrast to other rare-earth nitrides successful growth of EuN requires an activated nitrogen source. Synchrotron-based x-ray spectroscopy shows that the samples contain predominantly Eu^{3+}, but with a small and varying quantity of Eu^{2+} that we associate with defects, most likely nitrogen vacancies. X-ray absorption and x-ray emission spectroscopies (XAS and XES) at the nitrogen K edge are compared to several different theoretical models, namely, local spin density functional theory with Hubbard U corrections (LSDA + U), dynamic mean field theory (DMFT) in the Hubbard-I approximation, and quasiparticle self-consistent GW (QSGW) calculations. The DMFT and QSGW models capture the density of conduction band states better than does LSDA + U. Only the Hubbard-I model contains a correct description of the Eu $4f$ atomic multiplets and locates their energies relative to the band states, and we see some evidence in XAS for hybridization between the conduction band and the lowest-lying ^8S multiplet. The Hubbard-I model is also in good agreement with purely atomic multiplet calculations for the Eu M-edge XAS. LSDA + U and DMFT calculations find a metallic ground state, while QSGW results predict a direct band gap at X for EuN of about 0.9 eV that matches closely an absorption edge seen in optical transmittance at 0.9 eV, and a smaller indirect gap. Overall, the combination of theoretical methods and spectroscopies provides insights into the complex nature of the electronic structure of this material. The results imply that EuN is a narrow-band-gap semiconductor that lies close to the metal-insulator boundary, where the close proximity to the Fermi level of an empty Eu $4f$ multiplet raises the possibility of tuning both the magnetic and electronic states in this system.

DOI: 10.1103/PhysRevB.84.235120 PACS number(s): 71.55.Gs, 78.70.En, 78.70.Dm, 71.15.Mb

I. INTRODUCTION

The rare-earth nitrides (*R*Ns) display especially strong coupling between spin and charge degrees of freedom. They are thus of interest both as candidates for use in spintronics devices and as a fundamental testing ground for theories of the electronic structure of correlated materials.[1] Theoretical treatments predict that the series includes both half metals and ferromagnetic semiconductors.[2–7] However, treatment of the atomiclike $4f$ electrons within band theory is challenging, and the predicted electronic structures can be contradictory. Experimental investigations of the *R*Ns are also challenging, owing to the difficulty in preparing samples that are stoichiometric, and passivating them against oxidation in atmosphere. For most the magnetic state is known,[8,9] but much less information is available regarding the electronic structure. Recent progress has been made, especially in the case of GdN, with the demonstration of epitaxial film growth,[10–14] and studies of its electronic and magnetic properties.[15–21] Far fewer experimental data concerning the rest of the series are available.[22–26]

Of particular interest are the properties of EuN.[3,27–29] The ground state of the Eu^{3+} ion, the charge state anticipated when Eu bonds to nitrogen, has total angular momentum $J = 0$, so is nonmagnetic. However, the separate spin and orbital angular momenta are both large, and thus it is possible that magnetic ordering could exist in the form of "hidden ferromagnetism."[27] Accurate calculations of the electronic structure have proven difficult; for example, a treatment by local spin density functional theory with Hubbard U corrections (LSDA + U) that has been shown to be accurate for GdN (Refs. 3 and 17) was unable to determine whether EuN has Eu in the 2+ or 3+ charge state, due to the presence of Eu $4f$ states close to the Fermi level.[3] Thus, even the fundamental question of whether EuN is metallic or semiconducting remains unsettled.

There are presently few experimental studies that address the growth or electronic structure of EuN.[30–32] Recently, we reported an x-ray magnetic circular dichroism (XMCD) study of EuN thin films, which demonstrated that Eu is predominantly in the 3+ charge state, but that a small quantity (a few %) of Eu^{2+} is present in the films.[33] It appears that these 2+ ions are generated when low-lying empty Eu $4f$ levels become filled as a result of electron doping of the films, for example by nitrogen vacancies. The Eu^{2+} ions dominate the magnetic response, and the XMCD results raise the possibility that a sufficient density of 2+ ions could even support ferromagnetism against the Eu^{3+} background. More generally, such strongly localized levels close to the Fermi level can have a profound influence on conduction properties.[34–36] These considerations highlight the substantial

importance of developing theoretical techniques that can treat systems such as EuN.

Against this background we demonstrate epitaxial growth of EuN, and compare optical and x-ray spectroscopic data from the films with the predictions of several advanced electronic structure calculations, namely, LSDA + U,[3] quasiparticle self-consistent GW theory (QSGW),[6,37] and Hubbard-I[38,39] dynamic mean field theory (DMFT).[40,41] Each of the calculations brings a different perspective to the analysis of the electronic structure. Both the QSGW and DMFT calculations outperform the LSDA + U treatment in terms of accurately predicting the nitrogen p partial density of states (PDOS) measured by x-ray absorption and x-ray emission spectroscopies (XAS and XES, respectively). The results show that the previous LSDA + U calculations' prediction of a mixed Eu-f–Eu-d–like band near the Fermi level is an artifact of the difficulties in converging the LSDA + U calculations.

The QSGW calculation predicts a finite band gap, in agreement with optical spectroscopy, while the DMFT results, which rely on a LSDA + U calculation as input, predict a metallic band structure. On the other hand, the location of the Eu 4f levels, measured by XAS and x-ray photoelectron spectroscopy (XPS), is best captured by the DMFT method due to its more accurate treatment of the multiplet nature of the correlated 4f states. The combination of XAS and DMFT provides evidence for the existence of a low-lying Eu ^8S level close to the conduction band minimum. The picture of EuN that emerges is of a heavily doped semiconductor, where the interaction between extended band states and atomiclike 4f levels can lead to interesting physics.

II. COMPUTATIONAL METHODS

A. LSDA + U

The LSDA + U method as described by Larson *et al.*[3] was used here to obtain N p partial densities of states in the conduction band and compare them with the N K-edge XAS. The calculations are carried out using the full-potential linearized muffin-tin orbital (FP-LMTO) method.[42,43]

The LSDA + U method was originally developed by Anisimov *et al.*[44–47] as a way to deal with strongly correlated narrowband electrons in the framework of the Hubbard model. Essentially it comes down to a Hartree-Fock level treatment of the f states, in interaction with the other orbitals being treated at the usual orbital-independent local spin density functional approximation level. The double-counting terms are treated in the so-called fully localized limit.[45,48] What this means is that the total energies for the atomic limit of integer occupations of certain f sublevels agree between LSDA and LSDA + U. The LSDA + U calculation then essentially describes how these f-level occupations are adjusted self-consistently by their interactions with the other orbitals. The particular implementation used in this and the previous work by Larson *et al.*[3] is described by Liechtenstein *et al.*[47] and is formulated in terms of the density matrix of the f electrons.

An important issue is whether the LSDA + U solution is unique. Different starting-point density matrices may lead to different solutions, and in principle we need to pick the lowest-energy one. Larson *et al.*[3] found that in most rare-earth nitrides the optimum density matrix is close to obeying Hund's rules of maximal spin S_z and orbital angular momentum L_z. This solution breaks the cubic symmetry of the f states. On the other hand, EuN turned out to be one of the exceptions where a density matrix obeying cubic symmetry had lower energy. This is because the Hund's rule solution converged to an Eu^{2+}-like configuration by occupying the lowest empty f level of the Eu^{3+}. Similar convergence problems were mentioned by Johannes and Pickett,[27] although they were able to stabilize a Hund's-rule-obeying Eu^{3+} configuration with slightly different U parameters. Even within the solution obeying cubic symmetry, a band with mixed Eu f-d character was found to cross the Fermi level, predicting a metallic behavior. It is, however, not clear whether this metallic band would show up in transport because the mobility related to it might be low. The convergence problems in the LSDA + U treatment for EuN lead to a considerable uncertainty in this prediction. This uncertainty about the electronic structure of EuN makes it particularly interesting to study by spectroscopic methods and alternative theoretical treatments. In particular, we recognize that the problems have to do with the nature of the lowest empty f-like states, and these are not yet accurately described in full within LSDA + U theory because it lacks a proper treatment of multiplet splitting effects.

On the other hand, in Larson *et al.*'s LSDA + U treatment,[3] a U_d shift of the d bands is also included to open a band gap. This parameter was adjusted for GdN, but significant uncertainty exists in its values for other RNs such as EuN.

B. QSGW

The GW method is a many-body perturbation theory[49,50] for the self-energy of one-electron quasiparticle excitations. It is the first term in an expansion in terms of the screened Coulomb interaction W, schematically,

$$\Sigma(12) = iG(12)W(1^+2), \tag{1}$$

where $G(12)$ is the one-electron Green's function. Here, $1 = \{\mathbf{r}_1,\sigma_1,t_1\}$ is a shorthand notation for position, spin, and time, and 1^+ means $t_1 + \delta$. The one-electron Green's function provides the polarizability

$$\Pi(12) = -iG(12)G(21), \tag{2}$$

and hence the screening of the Coulomb interaction,

$$W(12) = v(12) + \int W(13)P(34)v(42)d(34). \tag{3}$$

Its accuracy depends on the starting independent-electron Hamiltonian H^0, which is usually taken as in the LDA. Its Green's function and the W constructed from it through the above equations are denoted G^0 and W^0. In the *quasiparticle self-consistent* or QSGW method,[37] the one-electron Hamiltonian H^0 from which G^0 is constructed uses an exchange-correlation potential,

$$v_{xc}^{QSGW} = \frac{1}{2}\sum_{nm} |\psi_n\rangle \mathrm{Re}[\Sigma_{nm}(E_n) + \Sigma_{nm}(E_m)]\langle\psi_m|, \tag{4}$$

which is itself extracted from the Σ of the previous iteration in such a way that the quasiparticle energies E_i, given by

$$\left[-\frac{1}{2}\nabla^2 + v_{\rm ext}(\mathbf{r}) + v_H(\mathbf{r})\right]\phi_i(\mathbf{r}) + \int \Sigma_{xc}(\mathbf{r},\mathbf{r}',E_i)\phi_i(\mathbf{r}')d^3r' = E_i\phi_i(\mathbf{r}), \quad (5)$$

and Kohn-Sham one-electron energies ϵ_i, given by

$$H_0\psi(\mathbf{r}) = \left[-\tfrac{1}{2}\nabla^2 + v_{\rm ext}(\mathbf{r}) + v_H(\mathbf{r}) + v_{xc}^{QSGW}\right]\psi_i(\mathbf{r}) = \epsilon_i\psi(\mathbf{r}), \quad (6)$$

approach each other upon self-consistency. In the above equations, $v_{\rm ext}$ is the external potential or interaction with the nuclei, v_H is the Hartree potential, and Re means taking the Hermitian part.

This approach, along with the specific implementation in terms of the full-potential linearized muffin-tin orbital method and a mixed basis set of product functions and interstitial plane waves, fully described in Refs. 51 and 52, was shown to give accurate band structures for a wide variety of systems.[37] In particular, for most semiconductors, it provides accurate but slightly overestimated values for the band gap. The remaining overestimate is related to the random phase approximation for the polarizability [Eq. (2)] and is in practice well taken into account by scaling the final Σ by a factor of 0.8. We will refer to this approximation as 0.8Σ.

Specifically for $4f$ electrons, however, it was found that the QSGW calculation significantly overestimates the energy of the empty f-electron states. This was shown for Gd metal, GdN, ErAs, etc.[6] Nonetheless, this appears to be unimportant for the band-gap region in GdN, which is accurately obtained. In practice, here for EuN, we take a LSDA + U calculation as the starting point but the final self-consistent QSGW result should, in principle, be independent of starting point.

C. DMFT

In spite of its accuracy for moderately correlated systems, the QSGW calculation still gives only the first term in a perturbation theory series. Essentially it still has a Hartree-Fock-like structure with a screened Coulomb interaction similar to the LSDA + U level of treatment of the f electrons. It does not yet take into account the more subtle correlation effects of the multiplet splittings of the f electrons. The latter arise from the different ways the electrons' orbital and spin angular momenta can combine to give different total angular momentum states in multideterminant wave functions. Such effects are mostly atomiclike and well understood since the work of Racah[53] and described, for example, in Condon and Shortley's book.[54]

A method for combining these atomic multiplet effects with band structure approaches is provided by the so-called Hubbard-I approximation[38,39] in dynamic mean field theory.[40,41] In these methods, the electronic structure of the localized orbitals is fully treated as a local decoupled impurity using atomic multiplet theory. The contributions of specific one-electron excitations between the multiplet states to the one-electron Green function are then calculated. These are expressed as a self-energy. This self-energy is now assumed to be independent of the Bloch wave vector $\mathbf{k}$ and is inserted in the Dyson equation for the crystal's Green's function with the coupling to other states turned back on. From this calculation, one obtains the hybridization of atomic-type multiplet excitations with the other states of the system. In the present paper, this calculation is carried out using a tight-binding atomic sphere approximation implementation[55] of the linearized muffin-tin orbital method.[56] This method is shown to represent the band structure of RNs similarly to the more accurate FP-LMTO method, provided adequate sphere sizes are chosen.[57] The parameters of the model include the on-site Coulomb interaction $U = 8.3$ eV as in the LSDA + U model, as well as atomic Slater integrals $F^2 = 13.5$, $F^4 = 8.45$, and $F^6 = 6.07$ eV. Spin-orbit coupling is included in the multiplet calculation at the intermediate coupling level. The final multiplet states can approximately be labeled by their ^{2S+1}L term label. The calculations consider the $f^6 \rightarrow f^7$ excitations reachable from the ground state term ^7F of the f^6 configuration by a single f-electron creation operator. This calculation is in principle most closely related to an inverse photoemission experiment, but as we will show it is also useful to interpret the M-edge XAS spectrum. Second, we calculate $f^6 \rightarrow f^5$ transitions and these are related most closely to photoemission.

D. Atomic multiplet theory

We have also carried out purely atomic multiplet calculations of the M_4- and M_5-edge XAS including a more complete atomic multiplet approach. In this approach, based on the computer codes reported by Thole *et al.*[58] the effects of the $3d$ core hole are included.

Thus, all initial state multiplets of the $d^{10}f^6$ and d^9f^7 configurations are calculated. Spin-orbit coupling is included and the calculation is carried out in the intermediate-coupling scheme. Calculations of the dipole-allowed optical matrix elements corresponding to $\Delta J = 0,1$ are carried out and produce a simulated spectrum. These calculations first of all provide a very different spectrum for Eu^{2+} and Eu^{3+} ions, and hence can be used as a fingerprint to determine the ratio of the contributions of these two valence states of the Eu in our samples. Second, however, the analysis provides us with approximate term labels of the initial and final state multiplets involved in each allowed transition as well as the labels of the corresponding pure f^7 parent term. We can thus attempt to correlate the present more complete atomic multiplet calculation of the XAS spectrum with the simpler DMFT f-only multiplet calculations described in the previous section. As these two portions of the work were carried out independently, slightly different atomic parameters were used. The Slater F^k integrals in this part of the work are given by $F^2 = 11.263$, $F^4 = 7.069$, and $F^6 = 5.086$ eV and the spin-orbit coupling parameter is 0.175 eV.

III. RESULTS

A. Epitaxial film growth

We begin by demonstrating epitaxial growth of EuN on [100]-oriented yttria-stabilized zirconia (YSZ). Figure 1 shows reflection high-energy electron diffraction (RHEED) images

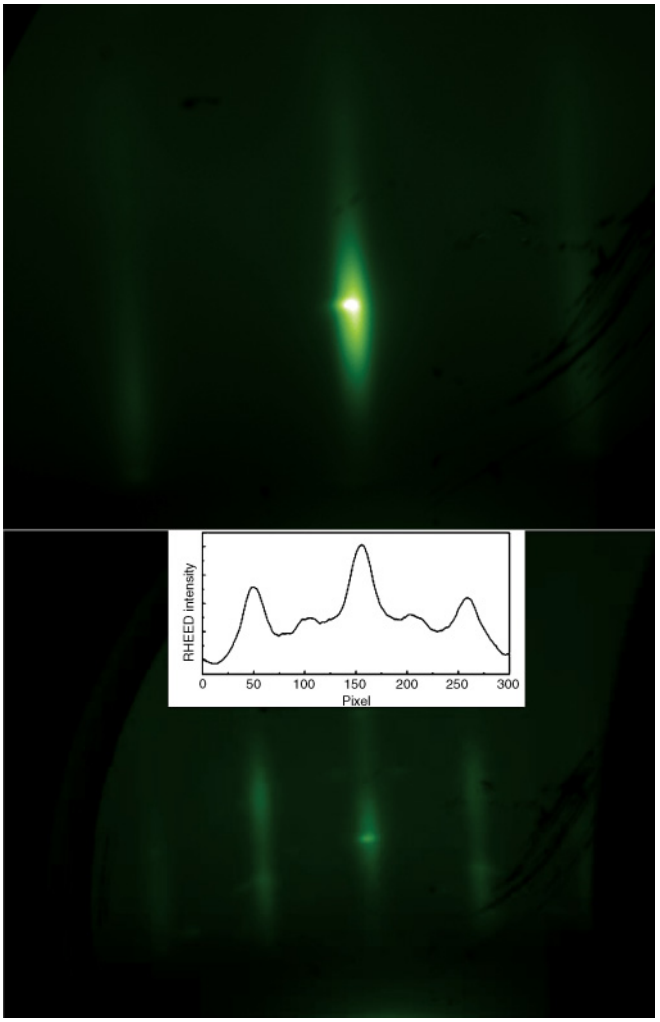

FIG. 1. (Color online) RHEED images from a 75-nm-thick epitaxial EuN film taken along (a) the ⟨100⟩ and (b) the ⟨110⟩ YSZ substrate azimuths. The film was grown at 590 °C, using 125 V N_2 ions from an ion source. The N_2 partial pressure was 3.7×10^{-4} mbar. The inset to (b) shows a line scan across the ⟨110⟩ pattern, emphasizing the weak streaks that suggest a surface reconstruction.

from a 75-nm-thick film grown at a substrate temperature of 590 °C in a Thermionics ultrahigh-vacuum system with a base pressure of 10^{-8} mbar. Eu metal (99.9% pure) was evaporated from a thermal source, and nitrogen supplied via an ion source producing 125 eV N_2^+ ions at a beam current of 0.24 mA. The overall N_2 partial pressure was 3.7×10^{-4} mbar. The film was grown at a rate of 0.4 Å/s after the YSZ substrate had been outgassed for 1 h at 600 °C. After growth the sample was capped with approximately 35 nm of AlN to allow *ex situ* studies without oxidation of the film in air. The streaky and rather narrow RHEED patterns are indicative of two-dimensional high-crystalline-quality epitaxial growth. Weak streaks lying between the main streaks along the ⟨110⟩ direction suggest that there may be a (2×1) surface reconstruction under these growth conditions [see Fig. 1(b) inset].

The x-ray diffraction pattern from this sample, shown in Fig. 2, exhibits intense peaks corresponding to the [200] and [400] reflections of rocksalt EuN. Unlabeled narrow features

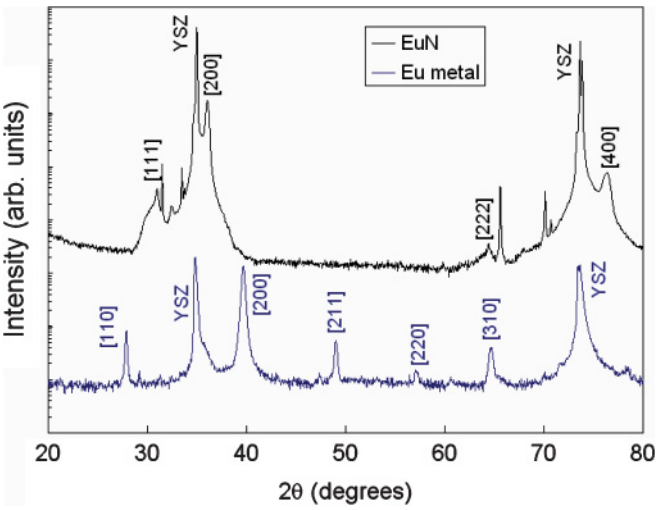

FIG. 2. (Color online) X-ray diffraction from an epitaxial EuN film grown using activated nitrogen from an ion source and from a film grown under similar conditions but without activated nitrogen. The latter contains only Eu metal.

correspond to substrate peaks that appear due to the slightly nonmonochromatic x-ray source. A [111] peak weaker than the [200] by about two orders of magnitude is observed at $2\theta = 64.3°$. There is an even weaker shoulder at about 30.3° indicating a small amount of EuO in the film, which may be associated with a thin oxide layer forming at the film/substrate interface due to mobile oxygen in the YSZ.[10] The measured EuN lattice constant is 4.98 Å, similar to the previously reported value of 5.02 Å,[30,31] and a Scherrer analysis of the peak widths indicates an ordered length scale of approximately 20 nm. The RHEED and x-ray diffraction results are comparable to those from the best gadolinium nitride films.[10–12,14]

A range of EuN samples have been grown under conditions similar to those described above, at temperatures between 475 and 590 °C, but a clear correspondence between growth temperature and film quality has not been established. In fact, not all samples grown under nominally similar conditions to the sample described above have yielded epitaxial growth, with some growths instead leading to films with a strong [100] texturing but no evidence of epitaxy in RHEED. Thus, growth of EuN appears to be sensitive to the growth conditions. We have also grown samples under the conditions described above, but without using the ion source. X-ray diffraction from one such sample, included in Fig. 2, exhibits peaks from metallic europium, but does not show clear EuN peaks. This provides evidence that growth of EuN using nitrogen gas requires that the nitrogen source be excited. This is in contrast to other rare-earth nitrides such as GdN, SmN, or DyN, which can be grown[22,59] under a partial pressure of nonexcited N_2, hinting at different chemistry involved in EuN growth.

B. XAS and XPS analysis of sample quality

To further analyze the growth mode and properties of EuN we have carried out XPS and XAS at the Soft X-ray Spectroscopy beamline of the Australian Synchrotron, and XPS, XAS, and XES at beamline X1B of the National

Synchrotron Light Source (NSLS) at Brookhaven National Laboratory, USA. At the Australian Synchrotron XAS data were recorded in total electron or fluorescence yield modes using the sample drain method or the intensity at a photodiode covered with an aluminum foil, respectively. XPS data were obtained with a SPECS Phoibos 150 Hemispherical Analyzer, with photon energies calibrated using Au $4f$ emission peaks. The incident photon energy resolution $\Delta E/E$ was about 1/5000, and the XPS resolution was about 0.3 eV. At the NSLS the XAS data were recorded in total electron yield mode using the sample drain method. The overall XAS resolution was about 0.2 eV at the N K edge and about 0.5 eV at the Eu M edge. XES data were measured using a Nordgren-type grazing-incidence soft x-ray spectrometer with resolution of about 0.4 eV at the N K edge. All data were obtained at room temperature. The XES and valence band XPS were calibrated by measuring the binding energy of the N 1s core level (396.6 eV; calibrated to the Fermi level using the known location of the $4f$ peaks of a gold reference sample).

For all synchrotron measurements samples were grown *in situ* at the synchrotron beamlines, thereby avoiding exposure of the samples to atmosphere and eliminating the need for a capping layer. At the Australian Synchrotron a thermal evaporator was used to evaporate the Eu onto YSZ [100] substrates, while nitrogen was introduced into the chamber via an ion source supplying 500 eV N_2^+ ions with a beam current of 7–10 mA. The partial pressure in the chamber was approximately 7×10^{-6} mbar. The Eu deposition rate varied from 0.2 to 0.5 Å/s, calibrated using a quartz crystal microbalance. The substrate temperature, estimated using a thermocouple, was approximately 550 °C for the first EuN growth (sample EuN^{AS}_{thin}) and 450 °C for the second (sample EuN^{AS}_{bulk}) (the former sample is substantially thinner than the latter, as described below). For comparison a film (sample $EuN^{AS}_{N_2}$) was grown at 450 °C with the ion source operating, but angled such that there was no line of sight to the substrate, thus allowing the role of the ion source to be investigated using films subject always to the same potential contaminants. A europium metal reference film was also grown at room temperature with no nitrogen added to the chamber (sample Eu^{AS}).

At the NSLS samples were deposited onto Si [100] substrates in a growth chamber with base pressure 2×10^{-8} Torr (properties of a representative sample EuN^{NSLS}_{bulk} are described below). The films were grown at a temperature of approximately 125 °C using a thermal evaporator for the Eu and an Oxford Scientific ECR plasma source for the nitrogen. The plasma source was run at about 21 mA and with a N_2 partial pressure of about 3×10^{-4} Torr. The Eu deposition rate was estimated to be 0.7 Å/s. A reference Eu metal film (sample Eu^{NSLS}) was prepared without introducing nitrogen to the chamber.

The europium M-edge x-ray absorption spectra of all samples are shown in Fig. 3. Also shown are calculated spectra for Eu^{2+} and Eu^{3+} ions obtained following Thole *et al.*,[58] as described in Sec. II D. All of the spectra are dominated by the expected Eu M_4 and M_5 absorption edges, with structure associated with multiplet levels. By comparison to the calculated spectra, we can conclude that the Eu metal sample Eu^{AS} is entirely Eu^{2+}, with no detectable presence

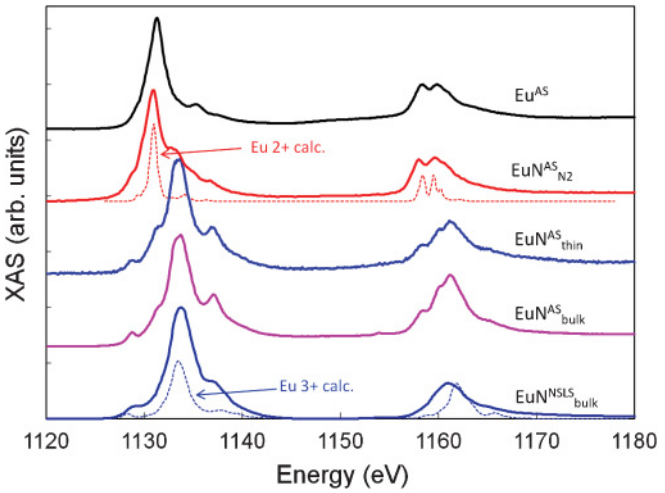

FIG. 3. (Color online) Normalized XAS taken over the Eu $M_{4,5}$ edges, compared to atomic multiplet calculations for Eu^{2+} and Eu^{3+} ions. Samples EuN^{AS}_{thin}, EuN^{AS}_{bulk}, and EuN^{NSLS}_{bulk} were grown using excited nitrogen, sample $EuN^{AS}_{N_2}$ under a nonexcited nitrogen partial pressure, and sample Eu^{AS} without nitrogen. Only EuN^{AS}_{thin}, EuN^{AS}_{bulk}, and EuN^{NSLS}_{bulk} contain predominantly Eu^{3+} corresponding to EuN, while $EuN^{AS}_{N_2}$ and Eu^{AS} are largely metallic Eu. Spectra are offset for clarity.

of Eu^{3+}. Similar results were obtained at the NSLS for the metallic sample Eu^{NSLS}. Sample $EuN^{AS}_{N_2}$, grown with the ion source occluded, displays only a weak contribution from Eu^{3+}, with the signal dominated by Eu^{2+}. Only the samples grown using an activated nitrogen source (samples EuN^{AS}_{thin}, EuN^{AS}_{bulk}, and EuN^{NSLS}_{bulk}) are dominated by Eu^{3+}. The only plausible candidates for the origin of the 3+ signal are EuN and Eu_2O_3, but if the latter were present significantly in samples EuN^{AS}_{thin} and EuN^{AS}_{bulk} we would also expect it in sample $EuN^{AS}_{N_2}$. Thus we attribute the Eu^{3+} to EuN, and conclude that Eu in EuN is predominantly in the 3+ charge state, and that, as found above, successful growth of EuN requires an excited nitrogen source.

The EuN samples EuN^{AS}_{thin}, EuN^{AS}_{bulk}, and EuN^{NSLS}_{bulk} also contain a small amount of Eu^{2+}, as evidenced by the small shoulder at about 1132 eV. We cannot firmly establish whether this is a result of metallic Eu inclusions in the films, or defects, such as nitrogen vacancies or residual oxygen, altering the Eu charge state. Most significantly, sample EuN^{NSLS}_{bulk} clearly contains the lowest Eu^{2+} concentration, so we conclude that it is the most close to stoichiometric of the films.

Nitrogen and oxygen 1s XPS were also measured for all samples. The nitrogen 1s XPS of sample EuN^{NSLS}_{bulk} shows a single dominant chemical environment, while the other samples show mixed chemical environments, further supporting our assessment that sample EuN^{NSLS}_{bulk} has the best quality of the films. All films showed the presence of some oxygen in as many as three different chemical environments, as signalled by core-level shifts of a few eV, which likely results from slight surface oxidation even under the low-pressure vacuum environment along with the incorporation of small amounts of oxygen during film growth. The surface sensitivity of XPS means the data may not be fully representative of the bulk of the films. Therefore we do not attempt to calculate the

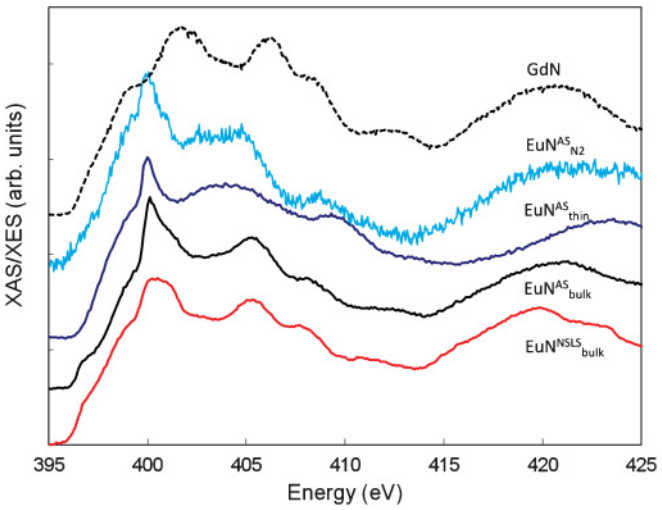

FIG. 4. (Color online) Normalized nitrogen *K*-edge XAS from a series of EuN samples grown under different conditions, along with the spectrum from GdN for comparison. The most nearly stoichiometric films are sample EuN^{NSLS}_{bulk} and sample EuN^{AS}_{bulk}, and these bear the most resemblance to the GdN spectrum. Note, however, the shoulder at about 397 eV that does not appear in GdN, and which is likely related to the presence of an Eu $4f$ multiplet near the conduction band minimum. Spectra are offset for clarity.

stoichiometry of the films or the impurity content based on XPS data, simply noting that the near-surface region of the films is clearly subject to some disorder.

More revealing are XAS and XES results obtained at the nitrogen *K* edge. XAS and XES are bulk probes (penetration depth ~50 nm), making them less sensitive to potential surface impurities, and they are element specific, picking out the partial density of empty (XAS) or filled (XES) states projected onto a nitrogen atom. Thus, to the extent that the electronic structure of EuN is influenced primarily by the local environment, these techniques are not directly influenced by impurities or off-stoichiometry. The nitrogen *K*-edge XAS from samples EuN^{AS}_{thin}, EuN^{AS}_{bulk}, and EuN^{NSLS}_{bulk} are shown in Fig. 4. We also include in the figure the XAS from GdN published previously.[22] The spectra have been aligned to the absorption onsets.

The most nearly stoichiometric film (sample EuN^{NSLS}_{bulk}) shows a structured XAS with clear peaks near 401 and 405 eV. Corresponding peaks can be identified in the GdN XAS at about 402 and 406 eV, and these have been shown to correspond to the t_{2g} and e_g crystal-field-split Gd $5d$ states, respectively.[18] This confirms the similar overall electronic structure of the two materials. The spectrum of sample EuN^{AS}_{bulk} displays the same main features as that of sample EuN^{NSLS}_{bulk}, but with an additional narrow peak near 400 eV that is most likely associated with molecular nitrogen trapped within the films, as seen also in disordered GaN films.[60] Sample $EuN^{AS}_{N_2}$, grown without direct exposure to the ion source, exhibits the same main spectral features as EuN^{AS}_{bulk} and EuN^{NSLS}_{bulk}, but with substantially worse signal-to-noise ratio due to the minimal incorporation of nitrogen into this film. Sample EuN^{AS}_{thin} shows a less structured XAS with a single broad peak near 404 eV rather than the clearly identifiable t_{2g} and e_g peaks seen in samples EuN^{AS}_{bulk} and EuN^{NSLS}_{bulk}. This sample is substantially thinner than sample EuN^{AS}_{bulk}, as demonstrated by strong substrate peaks visible in the XPS of sample EuN^{AS}_{thin}, which is likely a result of reevaporation of Eu at the higher growth temperature. The less structured XAS spectrum indicates a much larger degree of disorder in this film. Samples EuN^{AS}_{thin} and $EuN^{AS}_{N_2}$ both show evidence of molecular N_2. Overall, we conclude that sample EuN^{NSLS}_{bulk} is the most representative of bulk EuN, and below we single this sample out for comparison to theory.

C. Comparison of spectroscopies with theory

The nitrogen *K*-edge XAS from sample EuN^{NSLS}_{bulk} is compared in Fig. 5 with the N p PDOS in the conduction band calculated according to various models. As mentioned earlier, the LSDA + U calculations of Larson *et al.*[3] obtained two competing solutions for the f-electron density matrix. One started from Hund's rule Eu^{3+} but converged to a more Eu^{2+}-like solution. The other obeyed cubic symmetry and stayed Eu^{3+}-like but nonetheless was found to have an interesting hybrid f-d-like band crossing the Fermi level. This was found to be the lowest-energy state. We can see in Fig. 5 that neither of these models fits the nitrogen *K* edge well. Both overestimate the splitting between the t_{2g} and e_g peaks in the experiment, and the experiment does not show evidence for the low-energy peak near 394 eV that arises from the filling of the low f band and associated metallic character in this theory. On the other hand, the PDOS calculated in these models was taken to higher energy and does reasonably describe the peak in the 415–425 eV range.

The QSGW model is much better than LSDA + U at matching the experimental t_{2g}-e_g peak splitting, and the peak in the PDOS at 394 eV does not appear in this model. The DMFT PDOS also matches the N *K*-edge spectrum rather well.

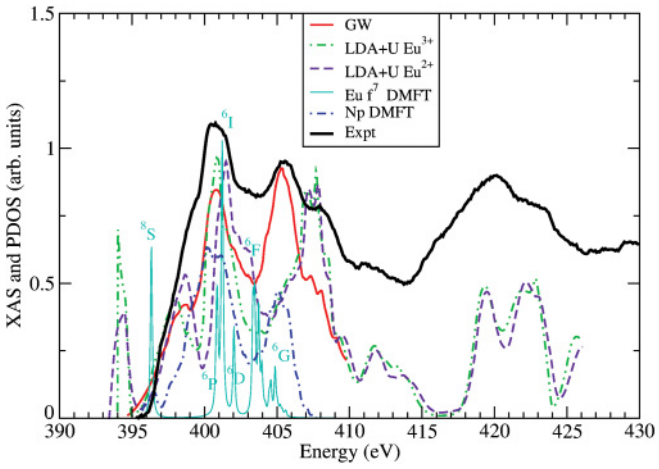

FIG. 5. (Color online) Various theoretical models of the N p projected density of states, compared with normalized nitrogen *K*-edge XAS and XES from sample EuN^{NSLS}_{bulk}. Thick black solid line, experimental data; green dash-dotted line and purple dashed line, LSDA + U for the cubic symmetry (Eu^{3+}) and Hund's rule (Eu^{2+}) solutions obtained by Larson *et al.* (Ref. 3); red solid line, QSGW results; blue dash-dotted line, DMFT calculation; turquoise thin solid line, Eu f PDOS in DMFT.

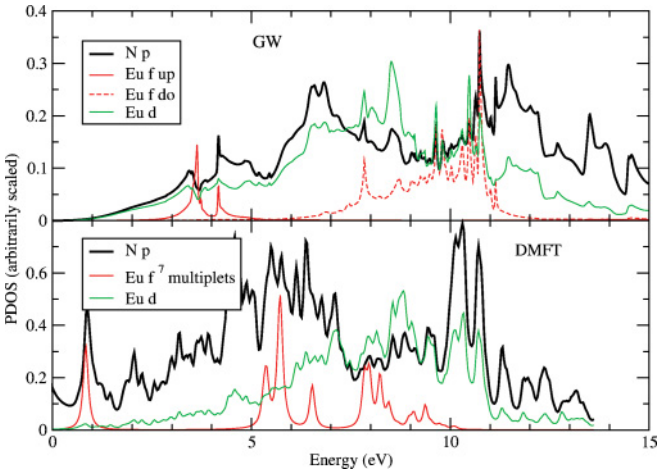

FIG. 6. (Color online) Partial density of states correlation in QSGW (upper panel) and DMFT (lower panel) calculations. For QSGW the Eu-f PDOS is resolved into spin-up (solid red line) and spin-down (dashed red line) components, whereas for DMFT a multiplet description is more appropriate.

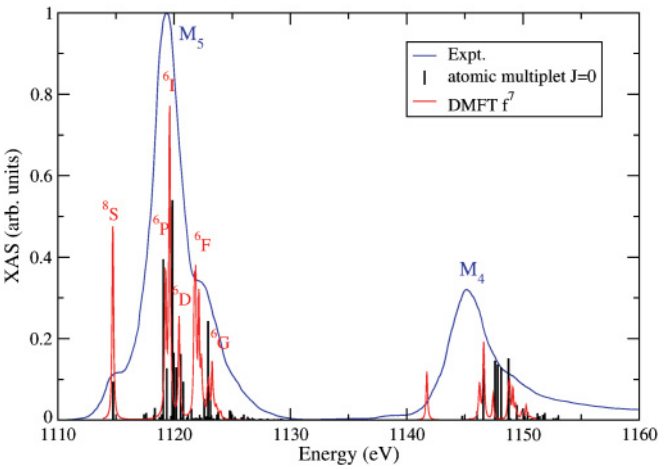

FIG. 7. (Color online) Comparison of Eu M_4 and M_5 XAS with DMFT and purely atomic multiplet spectra. Some of the main lines are labeled in spectroscopic notation.

The most notable difference between the QSGW and DMFT results is that the N p PDOS in DMFT shows a weak peak at about 396.5 eV. Comparison to the Eu f PDOS, also shown in Fig. 5, shows that this peak in DMFT is clearly correlated with the occurrence of the ^8S f^7 multiplet term of the Eu ion, and is thus evidence of hybridization of this state with the conduction band. Experimental evidence for this hybridization exists as a shoulder at about 397 eV in the spectrum of sample EuN^{NSLS}_{bulk}. A similar shoulder is clearly evident in sample EuN^{AS}_{bulk} (Fig. 4), but a corresponding feature is not seen in the GdN spectrum. That the experimental and theoretical peak energies do not perfectly match is because these energies in the theory depend on the precise choice of the U parameter and the Slater F^k integrals. Similar hybridization effects are also expected for the higher multiplet states but are more difficult to detect experimentally because they occur at energies where there is already a high spectral density.

To further examine hybridization effects, we compare in Fig. 6 the N p, Eu d, and Eu f PDOSs in both QSGW and DMFT calculations. One can see that there is a significant correlation between Eu d as well as Eu f and N p PDOSs. In QSGW, the conduction band is overall shifted up and the Eu f levels are separated into majority (up) and minority (down) spin. These are good quantum numbers in GW theory. In DMFT, on the other hand, the more accurate quantum number labeling in terms of the f^7 multiplet states is used. As described above, one may recognize that in particular the lowest high-spin ^8S multiplet occurs at low energy where the N PDOS is still weak, and therefore this feature can potentially be observed in the XAS spectrum.

A more direct way to detect the empty Eu f states is M-edge XAS. In Fig. 7 we compare the Eu M-edge XAS with both the DMFT theory and the atomic multiplet theory. Clearly, it is essential to take the multiplets into account. Neither LSDA + U nor GW contains this type of physics and thus they do not account for the f-level spectrum. The comparison of the atomic multiplet theory with the experimental spectra was already used as a fingerprint for the Eu^{3+}/Eu^{2+} ratio in Sec. III B. The point of interest here is to compare with the simpler DMFT multiplet theory that takes into account only the f levels and not the d core hole nor dipole matrix elements. We indeed see that the full multiplet theory and the f-only multiplet theory agree reasonably well with each other and with the XAS spectrum. This means that the complex multiplet splittings are in fact dominated by the f^7 multiplets and that the intensities are dominated by the degeneracies of these states rather than the intrinsic dipole matrix elements. In particular, we again note the low-energy ^8S peak, which clearly corresponds to the shoulder of the spectrum. The M_5-edge spectrum appears to be a somewhat better fit with the DMFT splittings than the M_4-edge spectrum. The atomic multiplet theory including the correct dipole matrix elements accounts better for the shape of the M_4 spectrum. The splitting between M_4 and M_5 is somewhat overestimated by the theory, indicating that the spin-orbit coupling of the $3d$ states is overestimated.

The main point about DMFT, however, is that this places the $4f$ multiplets relative to the other bands in the system, whereas the purely atomic multiplet theory is of course not capable of doing this. As was pointed out in the previous discussion, this allows us to study hybridization effects between N p and Eu f states.

We now turn to the occupied states as measured by XPS and XES and shown in Fig. 8. The XPS signal is heavily dominated by the Eu f states that provide a large peak centered at about -7.5 eV and a much smaller peak near -2.5 eV. The latter is associated with the small fraction of Eu^{2+} in the sample, and this unfortunately masks the signal from the N $2p$ valence band states. The XPS also shows a broad peak at about 20 eV binding energy (not shown) which is interpreted as the Eu $5p$ semicore level. If the XPS valence band maximum (VBM) is aligned with the N K-edge XES by a shift of 396.6 eV, we obtain good agreement of the various types of state with the DMFT theory. Although the XPS is too broad to fully resolve the f-multiplet splittings, we can clearly see the ^6P multiplet lines at lower energy as a high-binding-energy shoulder in the XPS spectrum. The energy of the Eu $5p$ states relative to the Eu f states matches reasonably well between theory and experiment. The Eu f states in LSDA + U (we use the cubic model here) lie

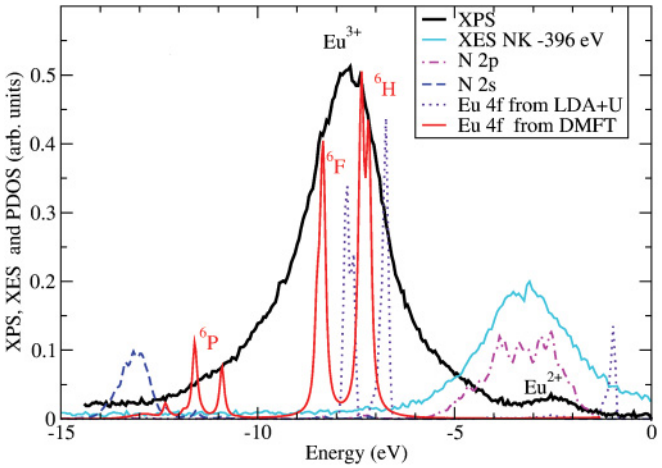

FIG. 8. (Color online) Comparison of XPS and XES measurements of the EuN valence band PDOS with various theories. Solid black line, XPS; thin light blue line, N K-edge XES; solid red line with labels, DMFT of Eu f^5 multiplet PDOS; blue dashed line, N $2s$ PDOS; pink dash-dotted line, N $2p$ PDOS; purple dotted line, Eu $4f$ in LSDA + U. The XES energy scale has been shifted by −396.6 eV.

more or less at the same energy below the VBM as those in DMFT, but again do not quite show the right splittings or locations to match the experimental data. Furthermore, there is no experimental evidence for the low-binding-energy partially occupied peak right at the Fermi energy that is characteristic of the LSDA + U model.

The N K-edge XES seen in Fig. 8 is not directly affected by contamination by Eu^{2+}, and it shows a shape that is consistent with that measured in other rare-earth nitrides.[18,22] As expected, the XES agrees well in shape with the calculated N p PDOS in either LSDA + U or GW theories.

To address the electronic state of EuN we have complemented the x-ray spectroscopies with optical transmittance measurements obtained at room temperature from the sample described in Sec. III A. As seen in Fig. 9, the transmittance is large at low energies, but shows a clear absorption onset near 0.9 eV, with the transmittance falling away toward the visible

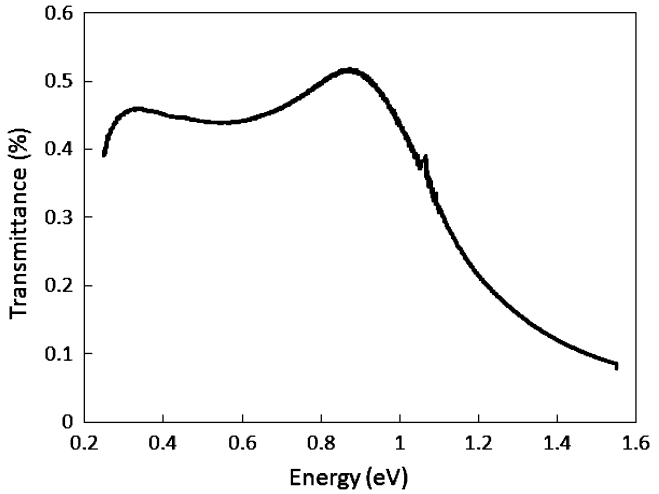

FIG. 9. Experimental optical transmittance of an epitaxial EuN film. The data show a clear absorption edge near 0.9 eV.

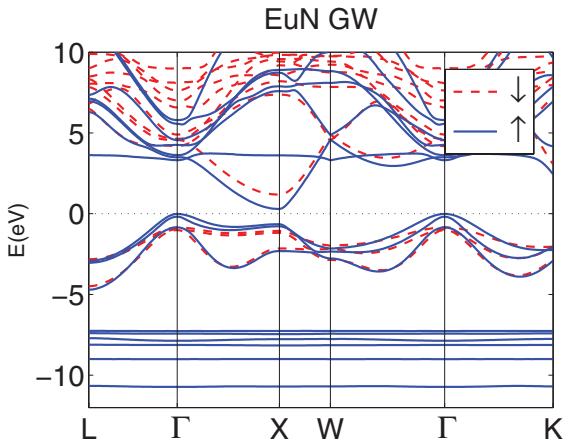

FIG. 10. (Color online) QSGW calculation showing a semiconducting band structure of EuN. The states are divided into majority (solid lines) and minority (dashed lines) spin states. The minimum gap at Γ-X is 0.31 eV, while the minimum direct gap at X is 0.94 eV.

end of the spectrum. The structure in the spectrum below 0.9 eV is related to interference effects associated with the finite thickness of the film and the capping layer, and the small feature just above 1 eV is instrument related. The existence of an absorption edge is suggestive of a semiconducting state for EuN with a finite band gap. However, optical absorption is dominated by direct transitions, whereas the minimum gap is expected to be between Γ and X in the band structure, as found previously for GdN.[17] We thus turn to an examination of the band structure calculated using QSGW theory, as shown in Fig. 10. The calculation does indeed return a semiconducting and ferromagnetic ground state, with a direct gap at X of 0.94 eV and a minimum indirect gap between Γ and X of 0.31 eV. The occupied majority-spin $4f$ levels are visible as relatively dispersionless bands from about −7 to −10 eV, with an unoccupied majority-spin band at about 4 eV that hybridizes somewhat with the conduction band. This lowest unoccupied $4f$ band is somewhat higher in energy than the ^8S multiplet level found in the DMFT calculation. Unoccupied minority-spin $4f$ levels are located above 7 eV. The spin polarization leads to exchange splitting between the majority- and minority-spin states that is especially evident near the band edges.

The majority-spin direct gap at X is quite similar in energy to the measured optical absorption edge. However, it is uncertain whether EuN could order ferromagnetically,[27] given the $J = 0$ ground state of the Eu^{3+} ion, and our measurements have found no evidence for such ordering at the temperatures used for the optical spectroscopy.[33] We have previously shown that for GdN the optical absorption edge in the paramagnetic state is reasonably well described by taking an average of the spin-down and spin-up direct band gaps.[17] Following this approach we obtain a spin-averaged direct QSGW gap at X of 1.59 eV for EuN, somewhat higher than the ferromagnetic (FM) gap and the optical absorption onset. However, the QSGW method is known to provide a slight overestimation of band gaps for many semiconductors.[37] It has successfully been applied to GdN,[6] for which it gives an indirect Γ-X majority-spin gap of 0.22 eV, while in the 0.8Σ approximation

it gives 0.05 eV for the indirect gap and a spin-averaged gap at X of 0.97 eV. Application of the 0.8Σ approximation to the present calculation would yield an averaged gap closer to the experimental absorption onset. On the other hand it may be that the spin-averaging approach is not valid here and the FM gap is closer to the paramagnetic gap.

In any case, like GdN, EuN appears to be very close to a metal-insulator transition with an almost zero indirect gap. Nevertheless, the results indicate that EuN lies on the semiconducting side of the transition under the conditions of our measurements. In contrast, for the DMFT calculation no attempt was made to adjust the d bands, and thus a clear overlap of the valence bands at Γ and conduction bands at X is obtained, in other words, a semimetallic band structure. The LSDA + U calculation does include a shift of the d bands, but it finds a band with mixed d and f character crossing the Fermi level and it thus predicts an actual metallic band structure.

IV. CONCLUSIONS

We have presented a detailed investigation of the electronic structure of EuN, drawing on both experimental results and a series of electronic structure calculations. We have demonstrated epitaxial growth of EuN, and have also shown using x-ray spectroscopy that the films typically contain a few atomic % of Eu^{2+} ions among the predominant Eu^{3+}. X-ray absorption, x-ray emission, and x-ray photoelectron spectroscopic data have been compared to the results of LSDA + U, quasiparticle self-consistent GW, Hubbard-I dynamic mean-field, and atomic multiplet calculations, with different aspects of the theories being emphasized in different energy ranges. The conduction band density of states measured by XAS matches the QSGW and DMFT results much better than it does the LSDA + U calculation. Our combined results make it clear that to understand the detailed features of the electronic structure it is essential to locate the atomiclike $4f$ multiplets relative to band features, and here DMFT is most able to capture the $4f$-electron physics. Of particular interest is the presence of a Eu ^8S f^7 multiplet level lying close in energy to the conduction band minimum. This offers the possibility of hybridization between conduction electrons and the atomiclike $4f$ states. We believe that it is this level that becomes occupied in substoichiometric EuN, leading to the small concentration of Eu^{2+} ions within the films. Optical absorption spectroscopy implies the presence of a direct band gap of around 0.9 eV at room temperature, which is most consistent with the QSGW band structure calculation, although the possibility remains that ferromagnetic EuN, if it exists, would have a small band overlap. Overall, the possibility of interacting conduction and $4f$ electrons and the presence of a small concentration of magnetic Eu^{2+} raises the possibility of complex and interesting physics in this material system.

ACKNOWLEDGMENTS

We acknowledge financial support from the NZ FRST (Grant No. VICX0808) and the Marsden Fund (Grant No. 08-VUW-030). The NSLS is supported by the US DOE Office of Basic Energy Sciences (Grant No. DE-AC02-98CH10886). The work at Case Western Reserve University and Boston University was supported by NSF Grant No. DMR-0710485. Parts of this research were undertaken on the Soft X-Ray beamline at the Australian Synchrotron, Victoria, Australia.

*ben.ruck@vuw.ac.nz

[1] B. J. Ruck, *Nanomagnetism and Spintronics: Fabrication, Materials, Characterization and Applications*, edited by F. Nasirpouri and A. Nogaret (World Scientific, Singapore, 2009), Chap. 9.

[2] C. M. Aerts, P. Strange, M. Horne, W. M. Temmerman, Z. Szotek, and A. Svane, Phys. Rev. B **69**, 045115 (2004).

[3] P. Larson, W. R. L. Lambrecht, A. Chantis, and M. van Schilfgaarde, Phys. Rev. B **75**, 045114 (2007).

[4] C.-G. Duan, R. F. Sabiryanov, J. Liu, W. N. Mei, P. A. Dowben, and J. R. Hardy, Phys. Rev. Lett. **94**, 237201 (2005).

[5] A. Sharma and W. Nolting, J. Phys.: Condens. Matter **18**, 7337 (2006).

[6] A. N. Chantis, M. van Schilfgaarde, and T. Kotani, Phys. Rev. B **76**, 165126 (2007).

[7] C.-G. Duan, R. F. Sabiryanov, W. N. Mei, P. A. Dowben, S. S. Jaswal, and E. Y. Tsymbal, J. Phys.: Condens. Matter **19**, 315220 (2007).

[8] F. Hulliger, in *Handbook on the Physics and Chemistry of Rare Earths*, edited by Karl A. Gschneider Jr. and LeRoy Eyring (North-Holland Physics Publishing, New York, 1979), Vol. 4, pp. 153–236.

[9] O. Vogt and K. Mattenberger, in *Handbook on the Physics and Chemistry of Rare Earths*, edited by K. A. Gschneider Jr., L. Eyring, G. H. Lander, and G. R. Choppin (Elsevier Science Publishers, New York, 1993), Vol. 17, pp. 301–407.

[10] B. M. Ludbrook, I. L. Farrell, M. Kuebel, B. J. Ruck, A. R. H. Preston, H. J. Trodahl, L. Ranno, R. J. Reeves, and S. M. Durbin, J. Appl. Phys. **106**, 063910 (2009).

[11] J. W. Gerlach, J. Mennig, and B. Rauschenbach, Appl. Phys. Lett. **90**, 061919 (2007).

[12] M. A. Scarpulla, C. S. Gallinat, W. S. Mack, J. S. Speck, and A. C. Gossard, J. Cryst. Growth **311**, 1239 (2009).

[13] T. B. Thiede, M. Krasnopolski, A. P. Milanov, T. de los Arcos, A. Ney, H.-W. Becker, D. Rogalla, J. Winter, A. Devi, and R. A. Fischer, Chem. Mater. **23**, 1430 (2011).

[14] F. Natali, N. O. V. Plank, J. Galipaud, B. J. Ruck, H. J. Trodahl, F. Semond, S. Sorieul, and L. Hirsch, J. Cryst. Growth **312**, 3583 (2010).

[15] F. Leuenberger, A. Parge, W. Felsch, K. Fauth, and M. Hessler, Phys. Rev. B **72**, 014427 (2005).

[16] F. Leuenberger, A. Parge, W. Felsch, F. Baudelet, C. Giorgetti, E. Dartyge, and F. Wilhelm, Phys. Rev. B **73**, 214430 (2006).

[17] H. J. Trodahl, A. R. H. Preston, J. Zhong, B. J. Ruck, N. M. Strickland, C. Mitra, and W. R. L. Lambrecht, Phys. Rev. B **76**, 085211 (2007).

[18] A. R. H. Preston, B. J. Ruck, W. R. L. Lambrecht, L. F. J. Piper, J. E. Downes, K. E. Smith, and H. J. Trodahl, Appl. Phys. Lett. **96**, 032101 (2010).

[19]K. Senapati, T. Fix, M. E. Vickers, M. G. Blamire, and Z. H. Barber, Phys. Rev. B **83**, 014403 (2011).
[20]N. O. V. Plank, F. Natali, J. Galipaud, J. H. Richter, M. Simpson, H. J. Trodahl, and B. J. Ruck, Appl. Phys. Lett. **98**, 112503 (2011).
[21]H. Yoshitomi, S. Kitayama, T. Kita, O. Wada, M. Fujisawa, H. Ohta, and T. Sakurai, Phys. Rev. B **83**, 155202 (2011).
[22]A. R. H. Preston *et al.*, Phys. Rev. B **76**, 245120 (2007).
[23]L. Degiorgi, W. Bacsa, and P. Wachter, Phys. Rev. B **42**, 530 (1990).
[24]C. Meyer, B. J. Ruck, J. Zhong, S. Granville, A. R. H. Preston, G. V. M. Williams, and H. J. Trodahl, Phys. Rev. B **78**, 174406 (2008).
[25]T. Komesu, H.-K. Jeong, J. Choi, C. N. Borca, P. A. Dowben, A. G. Petukhov, B. D. Schultz, and C. J. Palmström, Phys. Rev. B **67**, 035104 (2003).
[26]C. Meyer, B. J. Ruck, J. Zhong, S. Granville, A. R. H. Preston, G. V. M. Williams, and H. J. Trodahl, J. Magn. Magn. Mater. **322**, 1973 (2010).
[27]M. D. Johannes and W. E. Pickett, Phys. Rev. B **72**, 195116 (2005).
[28]M. Horne, P. Strange, W. M. Temmerman, Z. Szotek, A. Svane, and H. Winter, J. Phys.: Condens. Matter **16**, 5061 (2004).
[29]N. Kanoun-Bouayed, S. Goumri-Said, A. E. Merad, and M. B. Kanoun, Mater. Sci. Forum **609**, 167 (2009).
[30]W. Klemm and G. Winkelman, Z. Anorg. Allg. Chem. **288**, 87 (1956).
[31]C. Brown and N. J. Clark, J. Inorg. Nucl. Chem. **36**, 2507 (1974).
[32]R. Didchenko and F. P. Gortsema, J. Phys. Chem. Solids **24**, 863 (1963).
[33]B. J. Ruck, H. J. Trodahl, J. H. Richter, J. C. Cezar, F. Wilhelm, A. Rogalev, V. N. Antonov, B. D. Le, and C. Meyer, Phys. Rev. B **83**, 174404 (2011).
[34]A. C. Hewson, *The Kondo Problem to Heavy Fermions*, Cambridge Studies in Magnetism No. 2 (Cambridge University Press, Cambridge, 1997).
[35]H. Tsunetsugu, M. Sigrist, and K. Ueda, Rev. Mod. Phys. **69**, 809 (2009).
[36]S. Danzenbacher *et al.*, Phys. Rev. Lett. **102**, 026403 (2009).
[37]M. van Schilfgaarde, T. Kotani, and S. Faleev, Phys. Rev. Lett. **96**, 226402 (2006).
[38]A. I. Lichtenstein and M. I. Katsnelson, Phys. Rev. B **57**, 6884 (1998).
[39]S. Lebègue, A. Svane, M. I. Katsnelson, A. I. Lichtenstein, and O. Eriksson, Phys. Rev. B **74**, 045114 (2006).
[40]G. Kotliar, S. Y. Savrasov, K. Haule, V. S. Oudovenko, O. Parcollet, and C. A. Marianetti, Rev. Mod. Phys. **78**, 865 (2006).
[41]S. Y. Savrasov, K. Haule, and G. Kotliar, Phys. Rev. Lett. **96**, 036404 (2006).
[42]M. Methfessel, M. van Schilfgaarde, and R. A. Casali, in *Electronic Structure and Physical Properties of Solids: The Use of the LMTO Method*, edited by H. Dreyssé, Lecture Notes in Physics Vol. 535 (Springer Verlag, Berlin, 2000), p. 114.
[43]T. Kotani and M. van Schilfgaarde, Phys. Rev. B **81**, 125117 (2010).
[44]V. I. Anisimov, J. Zaanen, and O. K. Andersen, Phys. Rev. B **44**, 943 (1991).
[45]V. I. Anisimov, I. V. Solovyev, M. A. Korotin, M. T. Czyżyk, and G. A. Sawatzky, Phys. Rev. B **48**, 16929 (1993).
[46]V. I. Anisimov, F. Aryasetiawan, and A. I. Lichtenstein, J. Phys.: Condens. Matter **9**, 767 (1997).
[47]A. I. Liechtenstein, V. I. Anisimov, and J. Zaanen, Phys. Rev. B **52**, R5467 (1995).
[48]A. G. Petukhov, I. I. Mazin, L. Chioncel, and A. I. Lichtenstein, Phys. Rev. B **67**, 153106 (2003).
[49]L. Hedin, Phys. Rev. **139**, A796 (1965).
[50]L. Hedin and S. Lundqvist, in *Solid State Physics, Advanced in Research and Applications*, edited by F. Seitz, D. Turnbull, and H. Ehrenreich (Academic Press, New York, 1969), Vol. 23, pp. 1–181.
[51]M. van Schilfgaarde, T. Kotani, and S. V. Faleev, Phys. Rev. B **74**, 245125 (2006).
[52]T. Kotani, M. van Schilfgaarde, and S. V. Faleev, Phys. Rev. B **76**, 165106 (2007).
[53]G. Racah, Phys. Rev. **76**, 1352 (1949).
[54]E. U. Condon and G. H. Shortley, *The Theory of Atomic Spectra* (Cambridge University Press, Cambridge, 1953).
[55]O. K. Andersen and O. Jepsen, Phys. Rev. Lett. **53**, 2571 (1984).
[56]O. K. Andersen, Phys. Rev. B **12**, 3060 (1975).
[57]C. Mitra and W. R. L. Lambrecht, Phys. Rev. B **78**, 195203 (2008).
[58]B. T. Thole, G. van der Laan, J. C. Fuggle, G. A. Sawatzky, R. C. Karnatak, and J.-M. Esteva, Phys. Rev. B **32**, 5107 (1985).
[59]S. Granville, B. J. Ruck, F. Budde, A. Koo, D. J. Pringle, F. Kuchler, A. R. H. Preston, D. H. Housden, N. Lund, A. Bittar, G. V. M. Williams, and H. J. Trodahl, Phys. Rev. B **73**, 235335 (2006).
[60]B. J. Ruck, A. Koo, U. D. Lanke, F. Budde, S. Granville, H. J. Trodahl, A. Bittar, J. B. Metson, V. J. Kennedy, and A. Markwitz, Phys. Rev. B **70**, 235202 (2004).